SLAC – PUB – 3674 (REV.)
October 1985
(A)

LINEAR ACCELERATORS FOR TeV COLLIDERS*

P. B. WILSON
Stanford Linear Accelerator Center
Stanford University, Stanford, CA 94305

TABLE OF CONTENTS

* Work supported by the Department of Energy, contract DE–AC03–76SF00515.

Invited paper presented at the 2nd International Workshop on Laser Acceleration of Particles, Los Angeles, California, January 7–18, 1985

LINEAR ACCELERATORS FOR TeV COLLIDERS

P. B. WILSON
Stanford Linear Accelerator Center
Stanford University, Stanford, CA 94305

I. INTRODUCTION

This paper summarizes four tutorial lectures on linear electron accelerators which were presented at this Workshop:

1. "Electron Linacs for TeV Colliders" (P. B. Wilson)
2. "Emittance and Damping Rings" (P. M. Morton)
3. "Wake Fields: Basic Concepts" (R. K. Cooper)
4. "Wake Field Effects in Linacs" (K. L. F. Bane)

The first of these lectures was intended to introduce the general requirements for electron linacs capable of delivering beams for very high energy linear colliders. Material from this lecture is presented in the next three sections. Section II introduces the basic scaling relations for important linear collider design parameters. In Sec. III some basic concepts concerning the design of accelerating structures are presented, and breakdown limitations are discussed. In Sec. IV RF power sources are considered.

The fact that two of the four lectures were concerned with wake fields and their effects emphasizes the importance of this topic for high energy collider design. Several tutorial papers which give extensive coverage to wake field concepts and wake field effects have been published recently. No attempt will be made to duplicate this material here. Some key concepts will be discussed, and some examples of wake fields for typical linac structures will be presented in Sec. V. The reader is referred to the referenced literature for further study. The importance of emittance in linear collider design is also underscored by the scaling relations in Sec. II. Some general concepts concerning emittance, and the limitations on the emittance that can be obtained from linac guns and damping rings are discussed in Sec. VI.

In connection with Lectures 3 and 4, computer generated movies were shown at the Workshop which illustrated how wake fields arise as an electron bunch moves through typical structures, and how these wake fields in turn act on the bunch to produce emittance growth. Viewing such movies greatly enhances ones physical understanding of wake fields and their effects, but unfortunately this process cannot be reproduced on the printed page.

Finally, the author takes full responsibility for the manner in which the material presented by the other three lecturers has been condensed, summarized, or rearranged, and for all omissions and errors.

II. SCALING RELATIONS FOR LINEAR COLLIDERS

A. BEAM-BEAM PARAMETERS

Three parameters which characterize the interaction between two colliding bunches in a linear collider are the luminosity $\mathcal{L}$, the disruption D and the beamstrahlung δ. In the following, head-on collisions between tri–Gaussian bunches are assumed. The possibility of flat bunches crossing at a slight angle in the horizontal plane will be taken into account. The expressions given here for the three beam-beam parameters in the "classical" regime are taken from Refs. 1 and 2, where a more detailed discussion and additional references can be found.

LUMINOSITY

The luminosity (in $\mathrm{cm}^{-2}\ \mathrm{sec}^{-1}$) times the cross section (in cm^2) gives the event rate (per second) for any physical process taking place in the colliding bunches. Along with the beam energy, it is a primary design parameter for a linear collider. Assume identical e^+e^- linacs, each with energy $E_0 = eV_0 = \gamma mc^2$, pulsed at a repetition rate f and producing trains of b bunches per linac pulse. The luminosity is given by

$$\mathcal{L} = \frac{N^2 b f H_D}{4\pi\sigma_x\sigma_y} = \frac{N^2 b f \gamma H_D}{4\pi\epsilon_n \left(\beta_x^*\beta_y^*\right)^{1/2}} \quad . \tag{1a}$$

Here N is the number of particles per bunch, σ_y and $\sigma_x = R\sigma_y$ are the bunch height and bunch width (at the interaction point, unless otherwise indicated), $\varepsilon_n = \gamma\varepsilon_x = \gamma\varepsilon_y$ is the normalized emittance (assumed equal for each dimension), and β_y^* and β_x^* are the vertical and horizontal beta functions produced at the interaction point by the optics of the final focus system. If the disruption parameter is sufficiently large, the beams will pinch together as they pass through each other, producing an enhancement in the luminosity by a factor H_D. In practical units the luminosity is given by

$$\mathcal{L}\left(10^{32}\,\mathrm{cm}^{-2}\ \mathrm{s}^{-1}\right) = \frac{8.0\times10^{-6}}{R}\left\{\frac{b\left[N\left(10^{10}\right)\right]^2 f(Hz)\, H_D}{\left[\sigma_y(\mu m)\right]^2}\right\} \quad . \tag{1b}$$

DISRUPTION

The focusing effect produced by one beam acting on the particles in the other beam depends on the disruption parameter,

$$D = \frac{2r_0 N \sigma_z}{(1+R)\gamma\sigma_y^2} \quad . \tag{2a}$$

Here σ_z is the rms bunch length and r_0 the classical electron radius. Each beam acts like a lens with focal length σ_z/D for particles near the axis in the

opposing beam (if $D \lesssim 1$). For large values of D, the beams act like a plasma during the interaction, with the number of transverse plasma oscillations given[3] approximately by $(D/10)^{1/2}$. In practical units, the disruption parameter can be expressed as

$$D = \frac{.029}{1+R} \left\{ \frac{N\,(10^{10})\;\sigma_z\,(\mathrm{mm})}{E_0\,(\mathrm{TeV})\;[\sigma_y\,(\mu\mathrm{m})]^2} \right\} \quad . \tag{2b}$$

The luminosity enhancement as a function of D must be computed by a simulation. Results from simulations made to date differ somewhat in the maximum value of the enhancement H_D that can be obtained, and in the rate of rise of H_D as a function D near $D \approx 1$. Hollebeek[3] obtains a maximum enhancement ratio in the range five to six for $D \geq 1.5$. Fawley and Lee[4] find a maximum enhancement in the range three to four at $D \geq 3$. Some representative results from these two simulations are given in Table I below. For a flat beam with large aspect ratio, the enhancement ratio is given approximately by the square root of the round beam result. For intermediate values of the aspect ratio, the enhancement can be estimated from[5]

$$H_D(R) = H_D(1)\,\frac{R}{1+(R-1)\,[H_D(1)]^{1/2}} \quad . \tag{3}$$

Table I
Luminosity Enhancement as a Function of D

D	< 0.2	0.5	1.0	1.5	2.0	3	5
Hollebeek							
H_D (round)	1.0	1.4	3.6	5.2	5.6	5.9	6.0
H_D (flat)[a]	1.0	1.2	1.9	2.3	2.4	2.4	2.5
Fawley & Lee							
H_D (round)	1.0	1.0	1.5	2.2	2.6	3.1	3.4
H_D (flat)[a]	1.0	1.0	1.2	1.5	1.6	1.8	1.8

[a]Calculated assuming H_D (flat) $= [H_D\ (\mathrm{round})]^{1/2}$

BEAMSTRAHLUNG

We turn next to a consideration of the beamstrahlung parameter δ. As the colliding bunches pass through each other, the particles in one bunch are deflected by the fields in the opposing bunch. This transverse acceleration produces

synchrotron radiation, called beamstrahlung in this case. The beamstrahlung parameter δ is the average energy loss per particle, divided by the incident energy, calculated after the beams have separated. From the point of view of the physical processes occurring during the interaction between bunches, the relative energy loss in the center of mass system, $\delta/2$, is of more concern. The rms energy spread in the center of mass system may be somewhat less than $\delta/2$. Thus it is now conventional to take $\delta = 0.3$ as acceptable in collider design. However, it is well to remember that beamstrahlung is best studied by calculating the actual distribution function for the energy-loss, and this can only be done by a simulation in most cases of interest. The analytic expressions for δ which follow are, however, useful for scaling.

The expression for beamstrahlung in the classical regime (this term will be defined later) for two colliding tri–Gaussian bunches has been calculated by Bassetti and Gygi-Hanney:[6]

$$\delta_{c\ell} = \frac{r_0^3 N^2 \gamma}{\sigma_z \sigma_y^2} F(R) \quad , \tag{4a}$$

where $F(R)$ is a rather complicated function (see also Ref. 1) such that $F(1) = 0.22$ and $F(R >> 1) = 0.91/R^2$. Within a few percent, $F(R)$ is approximated by

$$F(R) \approx 0.22 \left(\frac{2}{1+R}\right)^2 \quad .$$

In the above calculation it was assumed that the particle trajectories do not change as the bunches collide. If the disruption parameter is large enough to cause the bunches to pinch, we would expect the beamstrahlung as well as the luminosity to be enhanced. This enhancement can be taken into account, at least approximately, by multiplying the preceding expression by H_D. A more exact beamstrahlung enhancement ratio can only be obtained by a simulation. In practical units Eq. (4a) becomes

$$\delta_{c\ell} \approx 1.0 \times 10^{-3} \left(\frac{2}{1+R}\right)^2 \left\{\frac{\left[N\left(10^{10}\right)\right]^2 E_0\ (\mathrm{TeV})}{\sigma_z\ (\mathrm{mm})\ [\sigma_y\ (\mu\mathrm{m})]^2}\right\} H_D \quad . \tag{4b}$$

The classical synchrotron radiation spectrum for a relativistic electron moving in a uniform magnetic field B peaks up near the critical photon energy $\hbar\omega_c = 3\hbar\gamma^2 eB/2mc$, in Gaussian units. However, when $\hbar\omega_c > \gamma mc^2$, one photon at the critical energy would have to carry more than the entire energy of the electron which emits it, and consequently the classical calculation of synchrotron radiation can no longer be valid. Define a scaling parameter Υ by

$$\Upsilon \equiv \frac{2}{3}\frac{\hbar\omega_c}{\gamma mc^2} = \gamma \frac{B}{B_c} \quad , \tag{5}$$

$$B_c \equiv \frac{m^2 c^3}{e\hbar} = \frac{e}{r_0 \lambda\!\!\!^{-}_c} = 4.4 \times 10^{13} \text{ G} \quad .$$

Here $\lambda\!\!\!^{-}_c$ is the Compton wavelength divided by 2π. For $\Upsilon \ll 1$ the classical calculation of the energy loss by synchrotron radiation is valid, while for $\Upsilon \gtrsim 1$ quantum effects, which act to reduce the energy of the emitted photons, must be taken into account. The modification of the synchrotron radiation spectrum by these quantum effects is summarized in Refs. 7 and 8. The rate at which an electron radiates energy in the quantum regime is reduced compared to the classical radiation rate. This reduction factor, H_Υ, is plotted in Fig. 1 as a function of Υ.

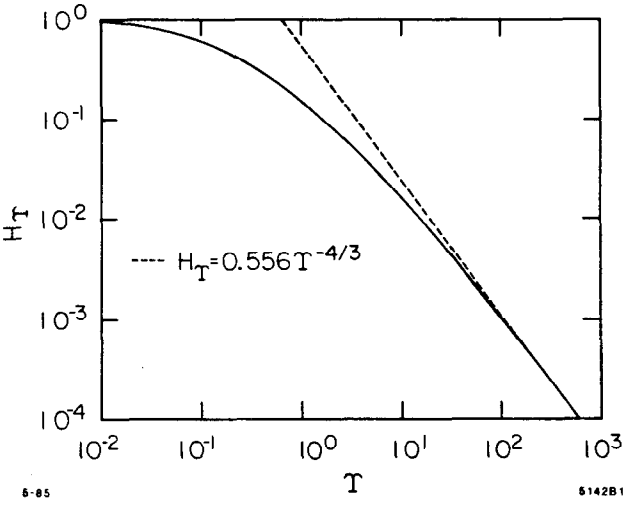

Fig. 1. Beamstrahlung reduction factor as a function of the scaling parameter Υ defined in Eq. (5).

An exact analytic calculation of the beamstrahlung parameter for Gaussian bunches in the quantum regime is difficult, and in any case a simulation must be carried out if the bunches pinch significantly. However, a rough approximation for scaling purposes is useful. We first compute the density-weighted average value of Υ for a flat beam. Assume the actual Gaussian bunch can be modeled by a particle distribution which is uniform in the longitudinal and transverse dimensions, having length $\sqrt{2\pi}\,\sigma_z$ and width $\sqrt{2\pi}\,\sigma_x$, respectively. Assume a Gaussian distribution in the vertical (narrow) dimension. The density-weighted average magnetic field is then

$$\overline{B} = \frac{0.50\,eN}{\sigma_x \sigma_z} = \frac{0.50\,eN}{R\sigma_y \sigma_z} \quad .$$

For a round beam we approximate the bunch by a particle distribution which is uniform over a length $\sqrt{2\pi}\,\sigma_z$ and Gaussian in the radial direction. The density-weighted average magnetic field is in this case

$$\overline{B} \;=\; \frac{0.29\,eN}{\sigma_y\sigma_z} \;\approx\; \frac{0.29\,eN}{\sigma_y\sigma_z} \quad .$$

Thus for any aspect ratio it is reasonable to approximate the average magnetic field by

$$\overline{B} \;\approx\; \frac{F\,eN}{2(1+R)\sigma_y\sigma_z} \quad ,$$

where F is a form factor of order unity. Substituting in Eq. (5), and doubling the result to take into account the effect of the electric field in the opposing bunch,

$$\overline{\Upsilon} \;\approx\; \frac{F\,r_0\,\lambda\!\!\!^{-}_c\gamma N}{(1+R)\sigma_y\sigma_z} \quad , \tag{6}$$

where $r_0\,\lambda\!\!\!^{-}_c = 1.09\times10^{-23}$ cm^2.[‡1] In practical units

$$\overline{\Upsilon} \;\approx\; \frac{2.1\times10^{-2}}{1+R}\left[\frac{N\,(10^{10})\;E_0\,(\mathrm{TeV})}{\sigma_z\;(\mathrm{mm})\;\sigma_y\;(\mu\mathrm{m})}\right]\;H_D^{1/2} \quad . \tag{7}$$

A factor $H_D^{1/2}$ has been included to account, very roughly, for pinch. Note from Fig. 1 that in the quantum regime H_Υ is given by $0.556\;\Upsilon^{-4/3}$. Using this together with Eqs. (2b), (4b) and (7),

$$\begin{aligned}\delta_Q \;&=\; \delta_{c\ell}\,H_\Upsilon \;\approx\; 6\times10^{-4}\left[\frac{DN\,H_D}{1+R}\right]^{1/3}\\ &=\; 1.25\left[\frac{DN\,(10^{10})\,H_D}{1+R}\right]^{1/3} \quad ,\end{aligned} \tag{8}$$

valid in the regime $\Upsilon \gtrsim 10$. From Eqs. (2b) and (4b) we also have

$$\delta_Q \;\approx\; 2.4\left[\delta_{c\ell}\,\frac{\sigma_z^2\;(\mathrm{mm})}{E_0^2\;(\mathrm{TeV})}\right]^{1/3} \quad . \tag{9}$$

---

‡1 In a recent simulation, R. Noble[5] finds $F \approx .86$ for Gaussian bunches if Eq. (6) is to be consistent with $\delta_Q = 0.556\;\delta_{c\ell}\Upsilon^{-4/3}$.

B. Beam Power and Wall Plug Power

The three beam-beam parameters discussed in the previous section depend only on the beam properties at the interaction point and the beam dynamics during the collision. A fourth parameter which is also independent of the accelerating linac is the beam power $P_b = bf\,N\,E_0$. For scaling purposes, we assume that all of the bunches in a train b bunches long accelerated during one RF pulse have the same charge and extract the same fraction of the energy stored in the accelerating structure. If there are, for example, eight bunches and each bunch extracts 4% of the stored energy, then this approximation is rather poor unless the bunch-to-bunch beam loading is compensated by one of several possible methods. As one example, the first bunch can be injected into a traveling-wave section before it is completely filled, and the spacing between bunches adjusted so that the energy added to the section between bunches just compensates for the bunch-to-bunch energy sag. In the following we assume this is done. It is also useful to introduce a normalizing voltage, current and power given by

$$V_n = mc^2/e = e/r_0 = 0.511 \text{ MV}$$

$$I_n = 4\pi V_n/Z_0 = ce/r_0 = 17.04 \text{ kA}$$

$$P_n = I_n V_n = ce^2/r_0^2 = 8.71 \text{ GW} \quad ,$$

where $Z_0 = 377\Omega$ is the impedance of free space. Thus

$$P_b' = \frac{P_b}{P_n} = \left(\frac{r_0}{c}\right) bf\,N\,\gamma \quad . \tag{10}$$

Of direct practical interest is the total "wall plug" power P_{ac} required by each linac in a collider. The wall plug power does depend on the properties of the accelerating structure. It is related to the beam power by $P_{ac} = P_b/(b\eta_{rf}\eta_s\eta_b)$, or per beam in practical units

$$P_{ac}\,(\text{MW}) = \frac{1.6\times 10^{-3}}{\eta_{rf}\eta_s\eta_b}\left[N\,(10^{10})\;E_0\,(\text{TeV})\,f\,(\text{Hz})\right] \quad . \tag{11}$$

Here η_{rf} is the efficiency for the conversion of ac power into rf power, η_s is a structure efficiency which takes into account the fact that some rf energy is dissipated in the structure walls during filling, and η_b is the fraction of the energy stored in the structure which is removed per bunch. If the rf pulse length T_p is made longer than the structure filling time T_f to compensate for bunch-to-bunch beam loading, as described above, then an additional efficiency given by T_f/T_p is required. In Sec. III A it is shown that a reasonable value for the net efficiency $\eta_{rf}\eta_s$ is, assuming some future technological improvements in the production of high peak power RF, $\eta_{rf}\eta_s \approx 0.5$. The single bunch efficiency is discussed below.

C. Single Bunch Efficiency and Energy Spread

The efficiency for energy extraction by a single bunch is

$$\eta_b = \frac{4eNk_1}{G} \quad , \tag{12}$$

where G is the accelerating gradient and k_1 is a structure constant given by

$$k_1 \equiv \frac{G^2}{4u} = \frac{C_0}{\lambda^2} \quad . \tag{13}$$

Here u is the stored energy per unit length, λ is the wavelength, and C_0 is a constant independent of wavelength which depends only on the structure geometry. For the SLAC disk-loaded structure, $C_0 = 2.1 \times 10^{11}$ V-m/C. It varies approximately as $(a/\lambda)^{-1}$, where a is the diameter of the iris opening[9]. Substituting Eq. (13) into Eq. (12),

$$\eta_b = \frac{4eNC_0}{\lambda^2 G} = 13.4 \, \frac{N\,(10^{10})}{\lambda^2\,(\mathrm{cm})\;G\,(\mathrm{MV/m})} \quad . \tag{14a}$$

This can also be written in Gaussian units for a linac of length L as

$$\eta_b = \frac{4\,r_0\,C_0'\,N\,L}{\lambda^2\;\gamma_f} = 93\,\frac{r_0\,N}{\lambda^2\,G'} \quad , \tag{14b}$$

where $G' = \gamma_f/L$, $k_1' = 0.21$ cm^{-2} and $C_0' = k_1'\lambda^2 = 23.2$ for the SLAC structure.

The single bunch energy spread is derived from the current distribution and the longitudinal wake potential, as described in Sec. V B. For a given accelerating structure and current distribution (*e.g.*, Gaussian), it is a function only of σ_z/λ, η_b and θ, where θ is the angle of the center of the bunch with respect to the crest of the accelerating wave. For the SLAC disk-loaded structure, the maximum value of η_b for a 1% and 2% single bunch energy spread (defined to include 90% of the bunch current) is given[10] in Table II below for several values of σ_z/λ. The angle θ ahead of crest has been chosen to minimize the energy spread. The effective accelerating gradient is reduced with respect to the peak unloaded gradient, both because the bunch is off crest and because there is a decelerating wake field within the bunch. The reduction factor in the gradient is given in the last column. The bottom row in the table shows that a very large single bunch efficiency can be reached if the bunch length is chosen so that shape of the bunch wake is approximately the inverse of the crest of the accelerating wave, as has been proposed at Novosibirsk.[11]

Table II
Maximum η_b for 1% and 2% Energy Spread

	η_b (%)		$\theta°$		E/E_0	
σ_z/λ	1%	2%	1%	2%	1%	2%
.005	2.3	3.2	29	45	0.85	0.66
.01	3.5	6.6	14	39	0.94	0.71
.02	–	6.5	–	8	–	0.94
.04	–	≈ 25	–	6	–	0.80

D. EMITTANCE GROWTH

Assuming a simple two-particle model for the bunch, several effects can cause the leading particle to drive the amplitude of the transverse oscillations of the tail particle as the bunch moves along the accelerator. To get a feel for scaling of emittance growth, consider the simplest case of a uniform machine with constant beta function, constant energy, and an offset x_0 in the leading particle at the beginning of the accelerator. From the results in Sec. VC, the amplitude of the oscillation of the tail particle at distance L, divided by the transverse size of the beam at the end of the machine, is

$$\frac{\Delta x_2}{\sigma_f} \approx \frac{1}{4} r_0 N L W_1 \left(\frac{\beta}{\gamma \epsilon_n}\right)^{1/2} x_0 \quad , \tag{15a}$$

where W_1 is the dipole wake at the tail particle due to the leading particle. In Gaussian units, $W_1 \approx 2 \times 10^5$ m^{-3} for the SLAC structure with $\sigma_z/\lambda \approx .01$. For a structure with constant geometry and fixed σ_z/λ, W_1 scales as $W_1 = C_1'/\lambda^3$, where $C_1' = 315$ for the SLAC structure geometry. Using this in Eq. (15a) and substituting η_b from Eq. (14b), we obtain

$$\frac{\Delta x_2}{\sigma_f} \approx \frac{C_1' \eta_b}{16 C_0'} \left(\frac{\beta\gamma}{\epsilon_n}\right)^{1/2} \left(\frac{x_0}{\lambda}\right) \quad . \tag{15b}$$

It is important to recall that the dipole wake constant C_1' depends on both the structure geometry and bunch length. Details are given in Sec. V.

A more realistic example assumes uniform acceleration from injection energy γ_0 to γ_f, with a beta function which varies as $\beta = \beta_0 \, (\gamma/\gamma_0)^{1/2}$. Assume also that the accelerator consists of M sections which are misaligned with an rms error d in transverse position. The the growth in amplitude of the tail particle

in the two particle model is then given by [12]

$$\frac{\Delta x_2}{\sigma_f} = \frac{1}{2} r_0 N L W_1 \left(\frac{\beta_f}{\gamma_f \epsilon_n}\right)^{1/2} \frac{d}{M^{1/2}} \quad . \tag{16}$$

Note that, in spite of the more complex assumptions, this result is still very similar to the simple scaling leading to Eq. (15a).

A third result has been obtained assuming uniform acceleration and constant beta function. Assume also a focusing lattice with a 90° phase advance per cell, with M focusing quadrupoles which jitter in transverse position with an rms displacement d. For this case the displacement of the trailing bunch grows to an amplitude[13]

$$\frac{\Delta x_2}{\sigma_f} = \frac{r_0 N L W_1}{2\pi} \left(\frac{\beta}{\gamma_f \epsilon_n}\right)^{1/2} M^{1/2} d \quad . \tag{17a}$$

Magnet misalignment is seen to impose a stricter limitation than accelerator section misalignment. For a 90° lattice the number of magnets is $M = 4L/\pi\beta$. Introducing also the gradient $G' = d\gamma/dz$, the preceding expression becomes

$$\frac{\Delta x_2}{\sigma_f} = \frac{r_0 N L W_1 d}{\pi^{3/2} \left(\epsilon_n G'\right)^{1/2}} \quad . \tag{17b}$$

By introducing an energy spread within the bunch (Landau damping), the emittance growth due to the dipole wake can be greatly reduced.[14] In Sec. V C it is shown that, for the simple case of a uniform structure having constant energy and beta function with an initial offset x_0, the growth in the transverse oscillation amplitude of the tail particle is reduced by a factor

$$\frac{\pi\beta}{2L(\Delta p/p)} \quad . \tag{18}$$

Thus Eq. (15a) becomes

$$\frac{\Delta x_2}{\sigma_f} = \frac{\pi r_0 N W_1 \beta^{3/2} x_0}{8 \left(\gamma \epsilon_n\right)^{1/2} (\Delta p/p)} \quad . \tag{19}$$

Landau damping is seen to be very effective in reducing emittance growth due to injection errors. It may be less effective in reducing the effect of alignment errors and magnet jitter, but detailed calculations remain to be done.

E. Design Strategy for Linear Colliders

Based on the relations summarized in the preceding sections, there are a number of ways to approach the design of a linear collider. We first assume that the energy, desired luminosity and allowable beamstrahlung are fixed. To carry this process further, some expressions which combine some of the preceding basic relations are useful. From Eqs. (1b) and (11),

$$\frac{\eta_{tot}\, P_{ac}\,(\mathrm{MW})}{E_0\,(\mathrm{TeV})\,[\mathcal{L}\,(10^{32})]^{1/2}} = 0.57\left[\frac{bfR\sigma_y^2\,(\mu\mathrm{m})}{H_D}\right]^{1/2} , \qquad (20)$$

where $\eta_{tot} = b\eta_b\eta_{rf}\eta_s = P_b/P_{ac}$. A reasonable upper value for η_{tot} is 0.15 (assuming $\eta_{rf}\eta_s = 0.5$, $b\eta_b \approx 0.3$). It is clear that the number of bunches, the repetition rate and the beam area $R\sigma_y^2$ should be chosen as low as possible to keep the AC power down. However, the constraint imposed by beamstrahlung must also be considered. From Eqs. (1b) and (4b),

$$\frac{E_0\,(\mathrm{TeV})\mathcal{L}\,(10^{32})}{\delta_{c\ell}} = 2.0\times 10^{-3}\left(\frac{1+R}{R}\right)^2 [bfR\sigma_z\,(\mathrm{mm})] \quad . \qquad (21a)$$

In order to get a high luminosity in the classical beamstrahlung regime, we see that, in contrast to the requirement set by Eq. (20) a large number of bunches and a high repetition frequency is desirable, as is a long bunch length. Since $\sigma_z = (\sigma_z/\lambda)\lambda$, this also implies a long RF wavelength. However, the aspect ratio R can be increased to allow reduced values of b, f and λ. In the quantum regime, the equivalent expression is, using Eq. (9) in Eq. (21a),

$$\frac{\mathcal{L}\,(10^{32})}{E_0\,(\mathrm{TeV})\,\delta_Q^3} = 1.5\times 10^{-4}\left(\frac{1+R}{R}\right)^2\left[\frac{bfR}{\sigma_z\,(\mathrm{mm})}\right] \quad . \qquad (21b)$$

It is seen that, contrary to the classical case, a short bunch length is helpful.

A final set of scaling relations is informative. Squaring Eq. (20) and dividing by Eqs. (21a) and (21b), we obtain

$$\frac{\delta_{c\ell}P_b^2\,(\mathrm{MW})}{E_0^3\,(\mathrm{TeV})\;\mathcal{L}^2\,(10^{32})} = 1.5\times 10^2\left(\frac{R}{1+R}\right)^2\frac{\sigma_y^2\;(\mu\mathrm{m})}{H_D\;\sigma_z\;(\mathrm{mm})} \quad , \qquad (22a)$$

$$\frac{\delta_Q^3P_b^2\,(\mathrm{MW})}{E_0\,(\mathrm{TeV})\;\mathcal{L}^2\,(10^{32})} = 2.2\times 10^3\left(\frac{R}{1+R}\right)^2\frac{\sigma_y^2\;(\mu\mathrm{m})\;\sigma_z\;(\mathrm{mm})}{H_D} \quad . \qquad (22b)$$

To see scaling more clearly, we can write these two relations in terms of the normalized emittance and β^* as

$$\frac{P_b^2\,(\mathrm{MW})\;\delta}{E_0^2\,(\mathrm{TeV})\;\mathcal{L}^2\,(10^{32})} = 2\times 10^{-2}\,\frac{H_\Upsilon\beta^*\,(\mathrm{mm})\;\epsilon_{\mathrm{n}}(\mu\mathrm{m}-\mathrm{rad})}{H_D\;\sigma_z\;(\mathrm{mm})} \quad , \qquad (22c)$$

$$\frac{P_b^2\,(\mathrm{MW})\;\delta_Q^3}{\mathcal{L}^2\,(10^{32})} \;=\; 0.3\;\frac{\sigma_z\;(\mu\mathrm{m})\;\beta^*\;(\mathrm{mm})\;\epsilon_n(\mu\mathrm{m}-\mathrm{rad})}{H_D} \quad . \qquad (22d)$$

Suppose $E_0 = 5$ TeV, $\delta = 0.3$, $\mathcal{L} = 10^{34}$, $P_{ac} = 100$ MW, and $\eta_{tot} = 0.15$ ($P_b = 15$ MW). Equations (22a) and (22b) then give

$$C\ell: \qquad \frac{\sigma_y^2\;(\mu\mathrm{m})}{\sigma_z\;(\mathrm{mm})} \;\approx\; 3.4\times 10^{-7}\;H_D\left(\frac{1+R}{R}\right)^2$$

$$Q: \qquad \sigma_y^2\;(\mu\mathrm{m})\;\sigma_z\;(\mathrm{mm}) \;\approx\; 5\times 10^{-8}\;H_D\left(\frac{1+R}{R}\right)^2 \quad ,$$

for the classical and quantum regimes respectively. Suppose $\sigma_z \approx 10^3\sigma_y$. Then in the classical and quantum regimes $\sigma_y \approx 3\times 10^{-7}$ μm and 5×10^{-3} μm, respectively. In both cases, one is forced to extremely small bunch dimensions.

When the bunch length has been chosen, the scale of the collider design has been set. Since σ_z/λ cannot be chosen arbitrarily, the choice of bunch length is related to a choice of operating wavelength. From Eqs. (22) the transverse dimension σ_y is now fixed (we have to guess initially whether we are in the classical or quantum regime, or else iterate on H_Υ in Eq. (22c). From Eq. (20) the product bfR is now fixed. It might be reasonable to choose $f = 360$. Some flexibility then remains in choosing b and R. The remaining quantities N, D, H_D, and $\overline{\Upsilon}$ are now readily calculated, and all parameters can be checked for consistency. It is left to the reader to continue this program for $E_0 = 5$ TeV, $\mathcal{L} = 10^{34}$ cm^{-2} and $P_{ac} = 100$ MW. It will be seen that for reasonable values of b, f and R, $\overline{\Upsilon} > 1$ and the parameters are pushed into the quantum regime.

III. ACCELERATING STRUCTURES

A. Structure Design

In this section we review a few basic expressions related to the design of traveling wave accelerating structures. Consider a periodic structure consisting of identical coupled cells with an RF feed at one end. For such a "constant impedance" structure, the group velocity v_g and attenuation per unit length are uniform along the length of the structure. The accelerating field is attenuated by a factor $e^{-\tau}$ along a structure of length ℓ, where

$$\tau \;=\; \left(\frac{\omega}{2Q}\right)\;T_f \quad , \qquad (23)$$

and $T_f = \ell/v_g$ is the filling time. Thus for a given τ, the filling time varies as $\omega^{-3/2}$. The structure efficiency, η_s, is defined as the ratio $V^2(\tau)/V^2(0)$, where

$V(\tau)$ is the actual voltage delivered by the structure and $V(0)$ is the voltage that would be obtained if the attenuation were zero. An input RF pulse with peak power P_0 and length T_f is assumed. Because of attenuation the energy per pulse required to reach a given accelerating gradient is increased by $1/\eta_s$. The structure efficiency is given by[15]

$$\eta_s = \left(\frac{1-e^{-\tau}}{\tau}\right)^2 \quad . \tag{24}$$

This function is plotted in Fig. 2. The efficiency is seen to approach 100% as $\tau \to 0$. On the other hand, the peak RF power required per unit length is

$$\frac{P_0}{\ell} = \frac{G^2}{r} f(\tau) \ , \tag{25}$$

$$f(\tau) = \frac{\tau}{2}\left(1-e^{-\tau}\right)^{-2} = \frac{1}{2\tau\eta_s} \ .$$

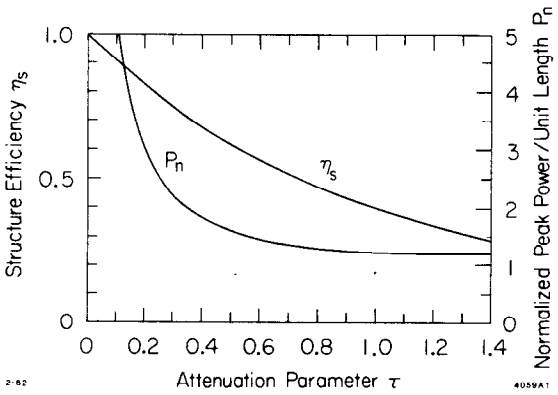

Fig. 2. Structure efficiency η_s and normalized peak power per unit length, $P_n = P_0 r/G^2\ell$, as a function of the attenuation parameter τ.

Here r is the shunt impedance per unit length and $G = V/\ell$ is the average accelerating gradient. Thus 100% efficiency ($\tau \to 0$) implies both zero filling time and infinite peak power. The function $f(\tau)$ has a minimum at $\tau = 1.26$, with f(1.26) = 1.23, as shown in Fig. 2. At this minimum, however, the efficiency is only 32%. By decreasing τ to 0.5, the efficiency is increased to 62% (almost double), while the peak power is increased by only 32%. Thus $\tau \approx 0.5$ gives a reasonable compromise between efficiency and peak power requirement. For the SLAC structure $\tau = 0.57$ and $\eta_s = 58\%$.

Present-day high power pulsed klystrons operate with a conversion efficiency of 45–55%. The efficiency for conversion of AC to DC pulsed power (modulator efficiency) is 80–90%. It is difficult to predict how much these efficiencies might be improved by future technological advances. A Lasertron[16] RF source operating directly from a DC power supply might, for example, achieve an efficiency on the order of 75%. Together with a structure efficiency of 65% ($\tau = 0.45$), this gives a possible net efficiency $\eta_{rf}\eta_s = 50\%$. An additional structure parameter is the loss parameter per unit length,

$$k_1 \equiv \frac{G^2}{4u} \tag{26}$$

where u is the stored energy per unit length. The factor of four comes from the fact that the loss parameter was originally defined by $u = k_1 q^2$, where u is the energy deposited in the accelerating mode per unit length by a point charge passing through a structure originally empty of energy. For a simple pillbox cavity of length g, the parameter k_1 is given by

$$k_1 = \left[0.456 \times 10^{12} \frac{\Omega - m}{s}\right] \frac{T^2}{\lambda^2} \quad ,$$

$$T = \frac{\sin \frac{\pi g}{\lambda}}{\frac{\pi g}{\lambda}} \quad .$$

We see from this expression, and directly from Eq. (26), that $k_1 \sim \omega^2$. For a SLAC type disk loaded structure with $\tau = 0.5$ and period $\lambda/3$,

$$k_1 = \frac{0.20 \times 10^{12}}{\lambda^2 \text{ (m)}} \frac{\Omega}{s - m} \text{ or } \frac{V}{C - m} \quad . \tag{27}$$

The SLAC structure doesn't do quite as well as a chain of simple pillboxes because of the finite disk thickness and field fringing in the disk aperture.

It is important to note that the value of k_1 depends strongly on the radius a of the disk aperture. This is shown in Fig. 3 for the SLAC structure. Approximately, $k_1 \sim a^{-1}$ for $a/\lambda \approx 0.1$.

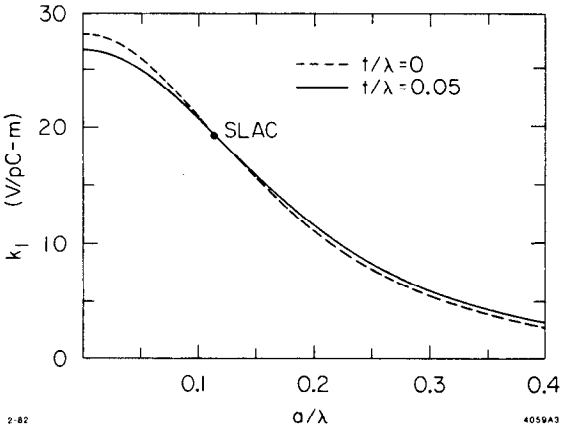

Fig. 3. Structure parameter k_1 as a function of beam aperture radius for the average cell in the SLAC disk-loaded structure ($\lambda = 10.5$ cm, $a = 1.163$ cm and $t = 0.584$ cm, where t is the disk thickness).

B. Peak Power Requirement

The filling time of a typical disk loaded accelerating structure with $\tau = 0.5$ will be 0.7 μs at $\lambda = 10$ cm [see Eq. (23)]. We can therefore write

$$T_f(ns) \;=\; 22\,[\lambda\ (\mathrm{cm})]^{3/2} \quad . \tag{28a}$$

The average energy per unit length required from a power source is

$$\bar{u}\left(\frac{J}{m}\right) \;=\; \frac{G^2}{4k_1\eta_s} \;=\; \frac{\lambda^2\ (\mathrm{cm})\ G^2\ (\mathrm{MV/m})}{5.0\times 10^3} \tag{28b}$$

for the same structure. The peak power requirement is

$$\frac{P_0}{L}\ (\mathrm{MW/m}) \;=\; \frac{\bar{u}}{T_f} \;=\; \frac{\lambda^{1/2}\ (\mathrm{cm})\ G^2\ (\mathrm{MV/m}))}{110} \quad . \tag{28c}$$

Results from Eqs. (28) are plotted in Fig. 4 for wavelengths from 1 mm to 10 cm and accelerating gradients from 50 to 500 MV/m.

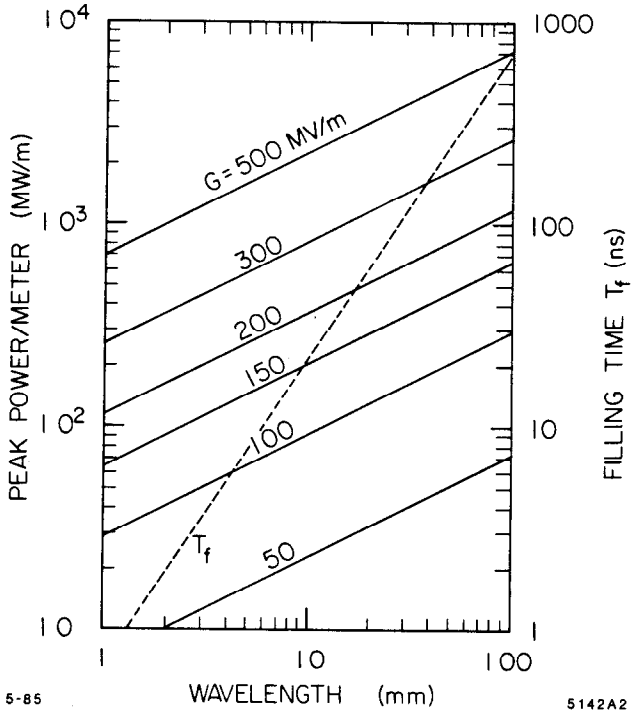

Fig. 4. Filling time and peak power per unit length as a function of wavelength for a typical disk-loaded structure with $\tau = 0.5$.

C. Limits on Accelerating Gradient

Several effects can impose limitations on the RF fields in an accelerating structure. The easiest to calculate and understand in simple physical terms is surface heating. The power per unit area absorbed by a surface with surface resistance R_s is

$$P_a = \frac{1}{2} R_s \hat{H}^2 = \frac{1}{2} G^2 \frac{R_s}{Z_s^2} \quad , \tag{29}$$

where $\hat{H}$ is the peak magnetic field and $Z_s = G/\hat{H}$ is an impedance defined by the geometry of the structure. For a typical disk-loaded structure, $Z_s \approx 400\Omega$. In terms of the power per unit area and the pulse length, T_p, the temperature rise is

$$\Delta T = \frac{2P_a}{K} \left[\frac{DT_p}{\pi}\right]^{1/2} \quad ,$$

where K is the thermal conductivity, $D = K/C_s\rho$ is the thermal diffusivity, C_s is the specific heat and ρ the density. Substituting for P_a from Eq. (29),

$$G = Z_s \left(\frac{K\Delta T}{R_s}\right)^{1/2} \left(\frac{\pi}{DT_p}\right)^{1/4} \quad . \tag{30}$$

If T_p is set equal to the filling time (which scales as $\omega^{-3/2}$), and since $R_s \sim \omega^{1/2}$, then $G \sim \omega^{1/8}$. Putting in typical numbers at $\lambda = 10$ cm for copper ($Z_s = 400\ \Omega$, $R_s = .014\ \Omega$, $K = 3.8$ W/cm–°K, $D = 1.1$ cm^2/s), and assuming also that the pulse length is equal to a typical filling time $T_p \approx 0.7\ \mu$s, then the gradient required to raise the surface to the melting point is $G \approx 1$ GeV/m. This model breaks down at $\lambda \approx 30\ \mu$m, when the diffusion distance $(DT_f)^{1/2}$ is on the order of the skin depth. Under this condition the filling time is about 5 ps and the gradient is about 2.6 GeV/m. For still shorter wavelengths, the temperature rise is determined only by the specific heat per unit volume, giving

$$\Delta T = \frac{P_a T_p}{\rho C_s \delta} = \frac{P_a T_p\ D}{K\delta} \quad ,$$

where δ is the skin depth. Substituting for P_a from Eq. (29),

$$G = Z_s \left(\frac{2K\lambda\Delta T}{\pi D Z_0 T_p}\right)^{1/2} \quad , \tag{31}$$

where $Z_0 = 377\Omega$. In this regime, G scales as $\omega^{1/4}$. Another limit is obviously encountered when the filling time becomes comparable to one rf cycle, $T_f \approx \lambda/c$. Also, at this limit a pulsed surface magnetic field can diffuse into the material a

distance equal to the skin depth in a time comparable to the filling time. Again scaling as $\lambda^{3/2}$ from $T_p = T_f \approx 0.7$ μs at $\lambda = 10$ cm, we find $\lambda = cT_f$ at $\lambda \approx 0.02$ μm. The gradient is on the order of 15 GeV/m, and $T_f \approx 10^{-16}$ sec.

The variation of gradient with wavelength due to surface heating is plotted for the different regimes in Fig. 5. A further discussion is given in the report of the Near Field Group, in these Proceedings.

The electric field limitations on gradient are less amenable to calculation. We expect the gradient limit to be a function of both frequency and pulse length. The well-known Kilpatrick criterion[17] predicts for CW or very long RF pulses,

$$E_b \text{ (MV/m)} \approx 25 \ [f \text{ (GHz)}]^{1/2} \quad , \tag{32}$$

for frequencies greater than a few GHz. Here E_b presumably can be taken as the peak field E_p at the surface of an accelerating structure, where typically $G \approx 0.5 E_p$.

The variation in breakdown field with pulse length is also not a precisely determined function. Some data[18] at 2856 MHz on the power flow at breakdown in a resonant ring, used at SLAC to test klystron windows, are fit by[♯2]

$$E_b\,(T_p) = E_b(cw) \left\{ 1 + \frac{4.5}{[T_p \ (\mu\text{s})]^{1/4}} \right\} \quad . \tag{33}$$

Combining Eqs. (32) and (33), for very short pulses

$$E_b \sim \omega^{1/2} \, T_p^{-1/4} \quad . \tag{34}$$

If the pulse length is equal to the filling time, and again assuming the filling time scales as $\omega^{-3/2}$, then $E_b \sim \omega^{7/8}$.

Two measurements have been made on breakdown in short resonant sections of disk-loaded structure near 3 GHz. Loew and Wang[20] at SLAC reached a peak surface field of 259 MV/m without breakdown at 2856 MHz for a pulse length of about 1.5 μs. Equations (32) and (33) predict a breakdown field of 215 MV/m. Tanabe[21] working at 2997 MHz, reports a peak field of about 240 MV/m at a pulse length of 4 μs, with some surface damage due to breakdown. If we use Eqs. (33) and (34) to scale these two results to a filling time of 0.7 μs at

♯2 The data can also be fit by a $(1+\text{const}/T_p^{1/3})$ variation. This scaling with T_p is in agreement with the behavior for DC pulses.[19] However, the enhancement factor over the Kilpatrick limit at S–band is then only a factor of three, which is inconsistent with experimental measurements.[20,21] If the $T_p^{1/3}$ variation is accepted, then the electric field breakdown limit plotted in Fig. 5 varies as ω^1 instead of $\omega^{7/8}$.

3 GHz, we obtain 310 MV/m for the Loew and Wang measurement, with no breakdown, and 350 MV/m for the Tanabe measurement, with breakdown and surface damage. As a calibration point on our plot of breakdown field versus wavelength, we therefore take 160 MV/m (assuming $G \approx E_p/2$) at $\lambda = 10$ cm. This is plotted in Fig. 5.

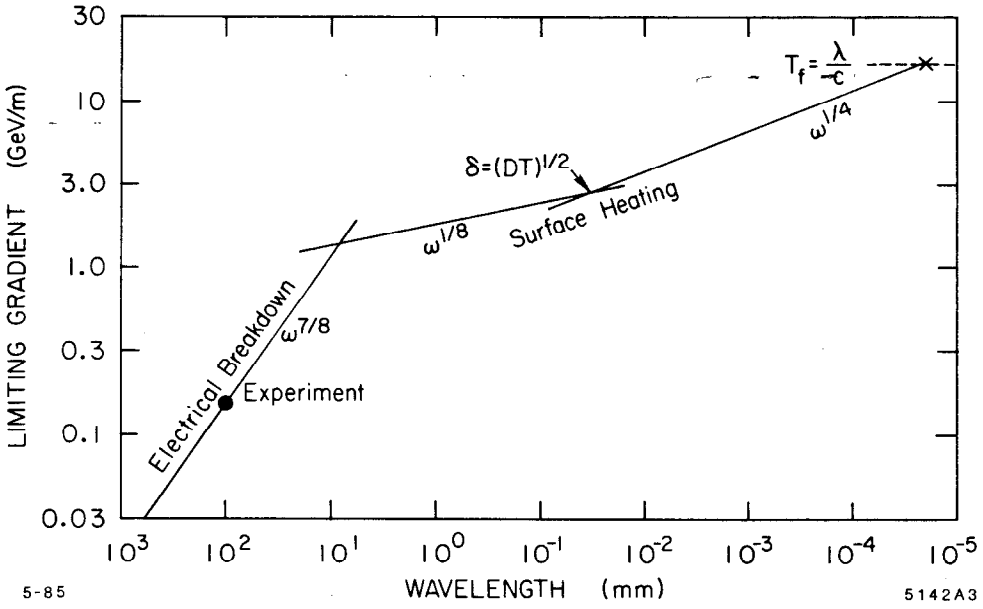

Fig. 5. Limitations on gradient as a function of wavelength due to electric field breakdown and surface heating in a SLAC–type disk-loaded structure.

IV. RF POWER SOURCES

A. General Remarks

From Fig. 4 we see that a collider linac operating at a gradient of (for example) 100 MV/m requires a peak power of 300 MW/m at $\lambda = 10$ cm and a peak power of 100 MW/m at $\lambda = 1$ cm. The pulse lengths for the two cases are about 700 ns and 20 ns, respectively. The required peak power can be generated either by external microwave tubes, or by a high current driving beam which can be external or internal to the accelerating structure. Further, the required peak power can be generated directly by the source at a pulse length equal to the filling time or alternatively at a lower peak power level and longer pulse length, followed by some pulse compression technique to raise the peak power to the required level. These alternatives are considered in the following sections.

RF sources which might be suitable for linear colliders are discussed in a recent review by Granatstein[22]. Sources which have produced peak power levels on the order of 100 MW in the wavelength range 1-10 cm are: virtual cathode oscillators (Vircators), backward wave oscillators, magnetrons, gyrotrons,

klystrons and free electron lasers. Oscillators, however, are not suitable as sources to drive a collider. Many amplifiers with good phase stability, driven from a common source, will be required. This reduces the possible sources to klystrons, gyrotron amplifiers (gyroklystrons), FEL's and possibly some type of crossed field amplifier. The latter device is a dark horse and will not be considered further. FEL's and other possible two-beam accelerators are considered briefly in Sec. IV D.

B. Klystrons and Gyroklystrons

For many years, klystron have been the RF source of choice for the highest peak power at wavelengths on the order of 10 cm. In 1970 a klystron was designed at $\lambda = 9$ cm to produce a peak power of 1 GW at $T_p = 15$ ns.[23] However, the tube failed before it could be tested at full output power. Recently, a klystron has been designed at SLAC to produce 150 MW at $\lambda = 10.5$ cm at a pulse length of 1 μs. This tube has now achieved[24] the design output power with an efficiency of 55%.

We have noted that a peak power of 300 MW/m is needed to reach an interesting accelerating gradient (100 MV/m) at $\lambda = 10$ cm. Also, it would be desirable to reduce the number of sources by spacing them further apart than 1 m. Furthermore, the optimum operating wavelength for a linear collider will almost certainly be shorter than 10 cm. It is difficult to specify a precise scaling law for the variation of peak power output of a klystron with wavelength, but almost certainly it will decrease more rapidly than the $\lambda^{1/2}$ requirement given by Eq. (28c). We conclude that some form of pulse compression will be needed if klystrons are used as an RF source for a linear colliders. If so, a premium will be placed on efficiency and reliability, rather than on peak power, assuming that a power level in the range 50–100 MW can be attained at the desired wavelength.

Gyroklystron are inherently capable of operating at shorter wavelengths than klystrons. For a collider operating in the wavelength range at or below 3 cm, a gyroklystron will probably be the RF source of choice (excluding for the moment two-beam concepts). Granatstein[25] has recently reviewed the capabilities of high peak power gyroklystrons. A design calculation has been made for a gyroklystron capable of delivering 300 MW at 9 GHz. This source would power two meters of typical structure at a gradient of 100 MV/m.

C. Lasertron RF Source

In recent years a new possibility for a high efficiency RF source has been the subject of increasing interest—the Lasertron. Figure 6 shows a schematic

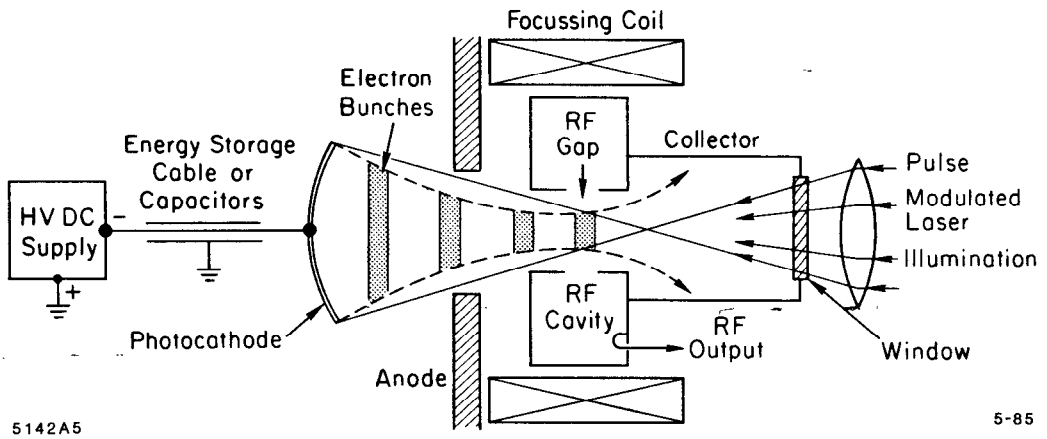

Fig. 6. Schematic diagram of a Lasertron RF power source.

diagram of this device. A laser beam, pulse modulated at the desired RF frequency, is incident on a photocathode. Electron bunches, each a small fraction of the RF period in length, are emitted by the cathode, accelerated to high voltage and passed through the gap of an RF cavity. If the RF voltage across the output gap is about equal to the DC beam voltage, each bunch is brought nearly to rest by the RF field in the gap, thereby converting DC to RF energy with very high efficiency. A further interesting feature of this device is that it can in principle by operated directly from a DC power source, eliminating the inefficiency associated with a pulse modulator. The laser-driven photocathode acts, in essence, as a switch operating at microwave frequencies, capable of the direct production of microwave power from a DC source.

Experimental work is currently underway on the Lasertron in Japan[26] and at SLAC[16]. At SLAC, a proof of principle test is underway to produce a Lasertron with a peak output power of 35 MW. Numerical simulations[27] indicate that an efficiency exceeding 70% is possible if a double output gap composed of two magnetically coupled output cavities is used. It is foreseen that peak power levels of 100 MW or more can be produced at a wavelength on the order of 10 cm. It is not so clear, however, whether this device can be scaled to produce high peak output power at substantially shorter wavelengths. Simulations are being carried out at SLAC to explore this possibility.

D. Pulse Compression

From the results of the preceding two section, it is seen that the direct generation of peak power level on the order of 300 MW/m by microwave tubes will be difficult, especially at shorter wavelengths. It should be emphasized again that it is also highly desirable to reduce the total number of RF sources by producing the required power level per meter from sources spaced at less frequent intervals. Thus some form of pulse compression and power splitting will

almost certainly be required for a very long collider operating at a high gradient. Suppose we require a gradient of 150 MV/m at a wavelength of 3.5 cm. From Fig. 4, this implies a peak power of about 400 MW/m. A filling time of about 125 ns is required. Suppose power sources are available capable of generating 100 MW for 1 μs. If the peak power can be multiplied by a factor of eight and split two ways, each source is then capable of feeding two meters of structure (assuming the pulse compression can be carried out with an efficiency close to 100%).

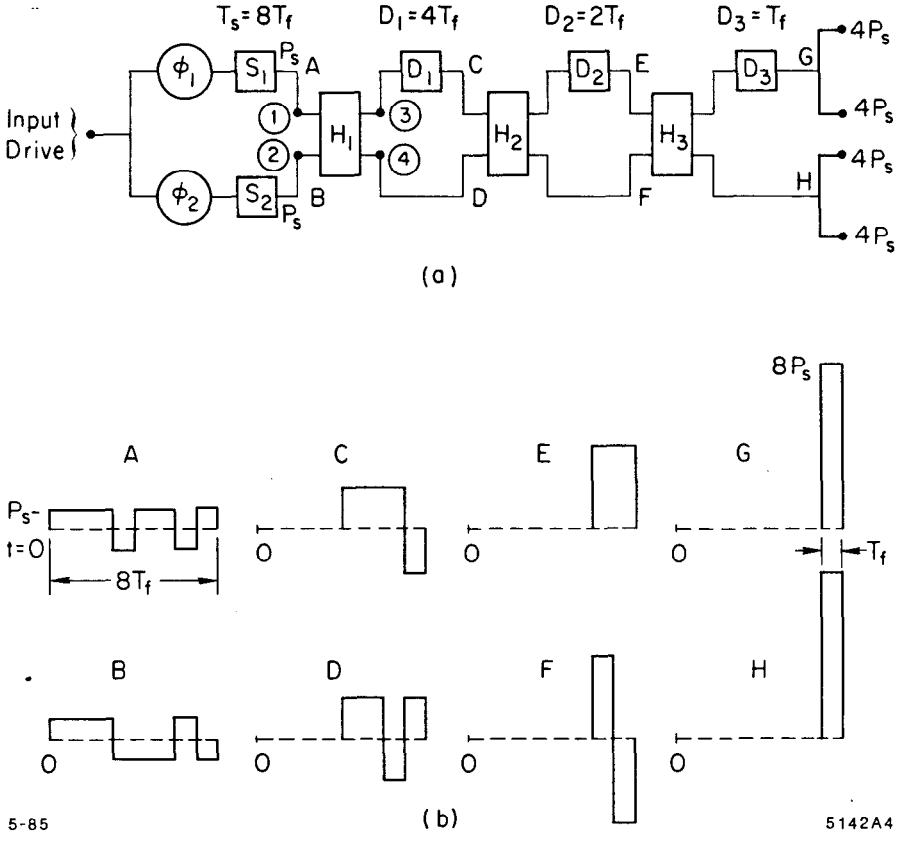

Fig. 7. (a) Diagram illustrating the pulse compression method of Z. D. Farkas;[28] (b) amplitude and relative phase of the RF power at the indicated points.

Figure 7a shows a method invented by Z. D. Farkas[28] for providing the desired pulse compression. Two RF power sources, S_1 and S_2, have a pulse length equal to eight time the structure filling time T_f. D_1, D_2 and D_3 are delay lines having, respectively, delays of $4T_f$, $2T_f$ and T_f. H_1, H_2 and H_3 are so-called 3db hybrids. If power is applied at either input terminal of such a device (terminal 1 or terminal 2 of H_1 for example), half the power appears at each output terminal (terminals 3 and 4 of H_1). There is, however, a 90° phase shift

between terminals 1 and 4 and between terminals 2 and 3. Thus, if the phase difference between the waves incident at terminals 1 and 2 is $\pm 90°$, it is readily seen by supposition that the combined power will appear at either terminal 3 or 4, depending on the sign of the phase difference. By changing the relative phase between the two input terminals by 180°, the power can therefore be switched from one output terminal to the other. By pulse coding the low power phase shifters ϕ_2 and ϕ_2 correctly in each of the eight time slots in the incident pulse, this switching is carried out in the hybrid H_1, H_2 and H_3 at increasing power levels and reduced pulse lengths. The process is illustrated in Fig. 7b, where the relative phase and power level is shown for the points indicated. The process can be extended, in principle, to any desired power multiplication by a factor of 2^n. Of course, the delay lines must not introduce significant attenuation. They can be either superconducting or over-moded room temperature copper pipes.

E. Two-Beam and Wake Field Accelerators

The energy per unit length required to produce an intense accelerating field can be produced by a variety of means other than by conventional external microwave power sources. An intense driving bunch, with appropriately shaped current distribution, can be injected on the axis of the accelerating structure ahead of the bunch to be accelerated (the collinear wake field accelerator).[29] A hollow ring-shaped driving bunch, which produces inwardly propagating wake fields in a suitable structure, can be used (the Voss-Weiland wake field accelerator).[30,31]

A low energy, high current beam moving in an external circuit parallel to the accelerating structure can be sent through a series of wigglers to generate the required RF power.[32,33] The energy lost by the driving beam is made up periodically by induction units. In addition to an FEL of this type, in which the parallel driving beam interacts with the transverse component of the RF field, a two-beam accelerator in which the driving beam interacts with a longitudinal RF field is also possible. In this device[34] a bunched beam, possibly produced by a laser-modulated photocathode, passes periodically through klystron-type cavities which extract a portion of the beam energy. The energy loss can again be made up by induction units. The disadvantage of this type of two-beam accelerator, in contrast to the FEL, is that the transverse dimensions of the RF interaction region must be comparable to the RF wavelength.

V. WAKE FIELDS

A. Delta Function Wake Potentials

The delta function wake $W(\tau)$ is the potential seen by a test charge following at a distance $c\tau$ behind a point unit charge passing through a component or structure. Both the test charge and the unit driving charge are usually assumed

to be travelling on parallel paths at the speed of light. The wake potential is then causal, such that $W(\tau) \equiv 0$ for $\tau < 0$. The instantaneous forces experienced by the test charge in response to the complex pattern of "wake fields" excited in even a simple structure are not usually of interest. What matters is the integrated force, or total potential seen by the test charge on passing through an entire component, or through one period of a periodic structure. The potential may be either longitudinal or transverse.

The theory underlying the wake potential description has been extensively developed in recent years. The analytic development is somewhat complex, with many subtleties. We give here only a few results of use in scaling wake field effects for relativistic particles in typical accelerating structures. The reader is referred to Refs. 35-38 for a more complete exposition.

The longitudinal wake field for the nth mode excited by a point charge q at radius r_q and azimuthal angle $\phi = 0$ in a cylindrically symmetric periodic structure is given by

$$E_z(r,\phi,\tau) \;=\; -2qk_n \left(\frac{r}{a}\right)^m \left(\frac{r_q}{a}\right)^m \cos m\phi \, \cos\omega_n\tau \quad . \tag{35}$$

Here $\underline{a}$ is the minimum wall radius of the structure (the disk hole radius), m gives the azimuthal dependence of the mode and

$$k_n \;\equiv\; \frac{E_{on}^2}{4u_n} \quad , \tag{36}$$

where u_n is the stored energy per unit length and E_{on} is the longitudinal synchronous field component at radius $r = a$. The delta function wake potential for the nth mode is now defined as the field per unit charge and per unit offset in both r_q and r at angle $\phi = 0$. Thus

$$\begin{aligned} W_{zn}(\tau) \;&=\; \frac{2k_n}{a^{2m}} \cos\omega_n\tau \quad , \\ E_{zn} \;&=\; -q\,W_{zn}(\tau)\, r^m\, r_q^m \cos m\phi \quad . \end{aligned} \tag{37}$$

The wake potential can also be defined as the potential per cell of the structure, rather than per unit length. In this case E_{on} and u_n in Eq. (36) are replaced by $\underline{E_{on}}p$ and u_np, where p is the periodic length. Note that the longitudinal wake for azimuthally symmetric ($m = 0$) modes is independent of the radial positions of both the driving charge and the trailing test charge.

To find the total wake potential behind a point charge for a given value of m, one must in principle sum over all possible modes supported by the structure with symmetry $\cos m\phi$,

$$W_z(\tau) = \frac{2}{a^{2m}} \sum_{n=1}^{\infty} k_n \cos \omega_n \tau \quad . \tag{38}$$

In practice a finite number of modes are calculated by an appropriate computer code, and an "analytic extension" is added to take care of the modes with frequencies above the limit of the calculation. The analytic extension is based on the fact that at sufficiently high frequencies the impedance $(dk/d\omega)$ can be shown to vary as $\omega^{-3/2}$ for typical accelerating structures.

The wake obtained by summing over 416 modes for the SLAC structure is shown by the dashed curve in Fig. 8 for 0–10 ps. Adding on an analytic extension gives the solid curve. The fundamental (accelerating) mode is also shown for comparison. Note that the total wake at $\tau = 0$ is about a factor of six greater than that given by the fundamental mode alone. The wake out to 300 ps is shown in Fig. 9.

If Fig. 8 shows the wake seen by a trailing test charge, one can ask what potential is seen by the driving (point) charge itself. It is easy to show[35] from conservation of energy that the potential

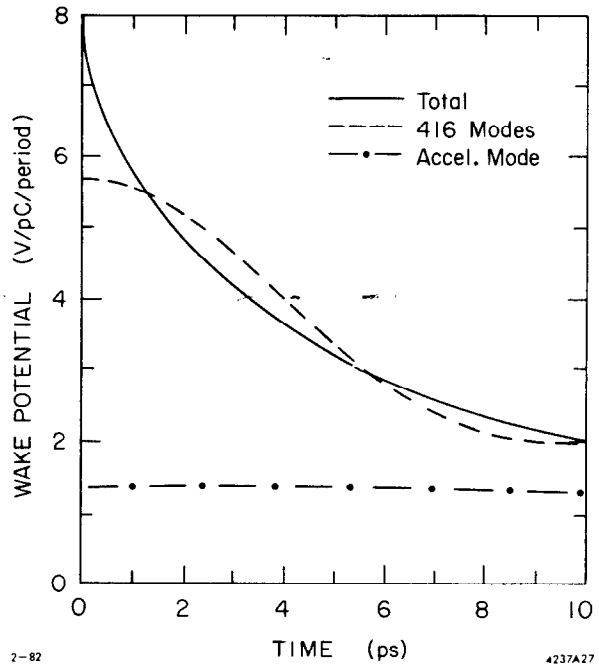

Fig. 8. Longitudinal wake potential per cell for the average cell in the SLAC disk-loaded structure in the range 0–10 ps.

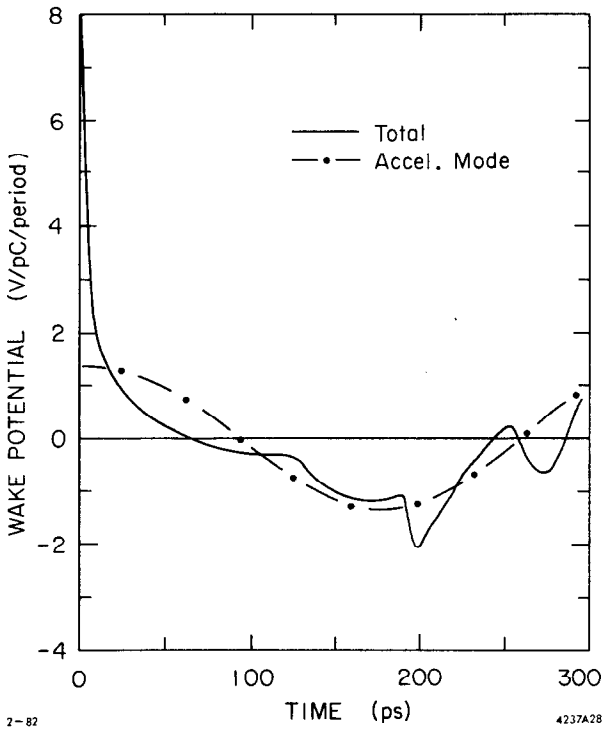

Fig. 9. Longitudinal wake potential per cell for the SLAC structure in the range 0–300 ps.

acting on the driving charge is just one-half of the wake potential seen by a test charge following an infinitesimal distance behind. Thus for the SLAC structure a point picocoulomb of charge experiences a retarding potential of 4 V per cell.

The transverse wake field is also of great interest for collider design. It is given, again for a single mode in a cylindrically symmetric periodic structure, by

$$\vec{E}_\perp(r,\phi,\tau) \;=\; 2qm\left(\frac{k_n c}{\omega_n a}\right)\left(\frac{r}{a}\right)^{m-1}\left(\frac{r_q}{a}\right)^m\left(\hat{r}\cos m\phi - \hat{\phi}\sin m\phi\right)\sin\omega_n\tau \quad , \tag{39}$$

where $\hat{r}$ and $\hat{\phi}$ we unit vectors. Here $e\vec{E}_\perp$ gives the total transverse force acting on the trailing particle. The delta function wake potential is now defined by

$$W_\perp(\tau) \;=\; \frac{2mk_nc}{\omega_n a^{2m}}\sin\omega_n\tau \quad , \tag{40}$$

and

$$\vec{E}_\perp \;=\; qW_\perp(\tau)\,r^{m-1}\,r_q^m\left(\hat{r}\cos m\phi - \hat{\phi}\sin m\phi\right) \quad .$$

For the important case of the dipole ($m = 1$) modes, the deflection field varies linearly with the offset of the leading charge and is uniform across the entire aperture of the structure behind the leading charge. Note that the wake potentials W_z and $W_\perp$ are scalar function of τ only. We see also that the longitudinal and transverse wake fields are related by

$$\frac{\partial\vec{E}_\perp}{\partial\tau} \;=\; -c\,\nabla_\perp E_z \quad . \tag{41}$$

The total delta-function wake potential is again obtained by summing over many modes and adding an analytic extension as described in Ref. 35. Results for the dipole mode for the SLAC structure are shown in Figs. 10 and 11. Note that, in contrast to the longitudinal wake, the dipole wake (and all transverse wake potentials) starts at zero at time $\tau = 0$ and rises to a first maximum at a distance behind the driving charge which is comparable to the iris aperture radius. At long distances behind the driving charge, the total wake is given by a beating of the wakes due to the two or three lowest frequency modes. The period of the resulting semi-regular oscillation is substantially that of the lowest frequency mode.

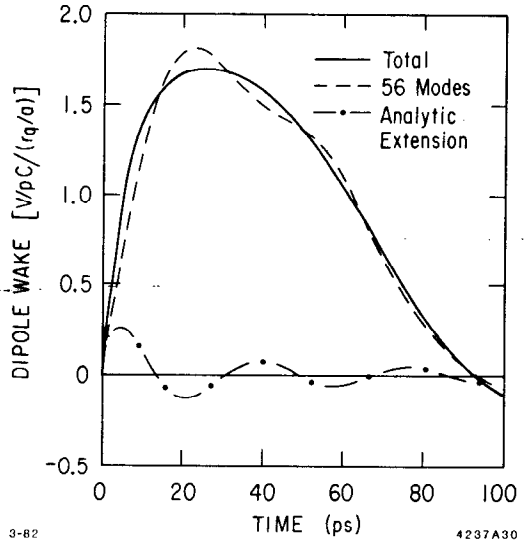

Fig. 10. Dipole wake potential per cell for the average cell in the SLAC disk-loaded structure in the range 0–100 ps.

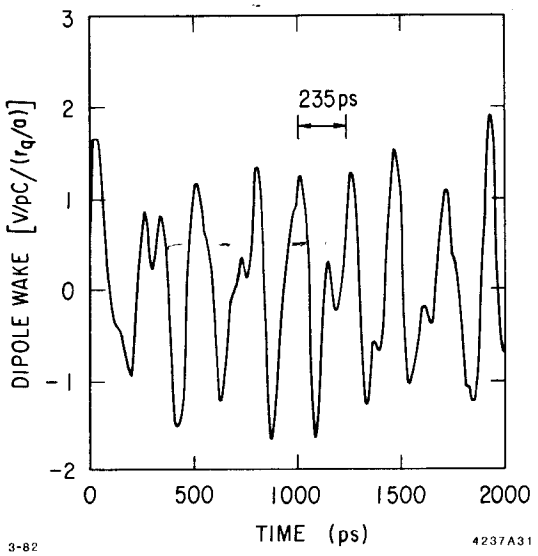

Fig. 11. Dipole wake potential per cell for the SLAC structure in the range 0–2000 ps. The period of the lowest frequency dipole mode is 235 ps.

From Eq. (36) it is seen that $k_n \sim \omega^2$. Thus from Eqs. (37) and (40) the wake potentials per unit length scale as

$$\begin{aligned} W_z^m &\sim \omega^{2m+2}, \qquad m \geq 0 \\ W_\perp^m &\sim \omega^{2m+1}, \qquad m > 0 \quad . \end{aligned} \tag{42}$$

The wake potentials per cell of a periodic structure scale as one power lower than above. The horizontal time axes in Figs. 8–11 also scale, of course, in proportion to the wavelength.

The above scaling is for a constant geometry such that all dimensions vary in proportion to wavelength. The case in which only the disk hole radius is varied for a structure of fixed frequency is also of interest. This scaling has been investigated for the SLAC structure by K. Bane[39]. The intercept at $\tau = 0$ for the longitudinal wake is found to vary as

$$W_z(0) \sim a^{-1.7} \quad . \tag{43a}$$

The time at which the longitudinal wake falls to one-half of its value at $\tau = 0$ is given by

$$c\tau_{1/2} \approx .09\,a \quad . \tag{43b}$$

The amplitude of the first maximum of the dipole wake is found to vary with beam aperture radius as

$$W_1(\tau_m) \sim a^{-2.25} \quad , \tag{43c}$$

where the value of τ_m varies as

$$c\tau_m \approx 0.65\,a \quad . \tag{43d}$$

The initial slope of the dipole wake for $\tau << \tau_n$ varies as

$$\frac{dW_1}{d\tau} \sim a^{-3.5} \quad . \tag{43e}$$

Finally, a note about dimensions. In the scaling relations developed in Sec. II, it was found to be convenient to use *cgs*–Gaussian units. The wake potentials per particle in *cgs* units are readily obtained from the potential per unit charge in *mks* units by multiplying by $4\pi\epsilon_0$. Thus the $m = 0$ longitudinal wake potential per unit length, with dimension $V/(C-m)$ in mks units, has dimensions $1/\mathrm{m}^2$ (or $1/\mathrm{cm}^2$) in Gaussian units. We have, in general, for the wake potential per unit length

		mks	Gaussian
$m = 0$	W_z	$\frac{V}{C-m}$	$\frac{1}{m^2}$
$m = 1$	$W_\perp$	$\frac{V}{C-m^2}$	$\frac{1}{m^3}$
	W_z	$\frac{V}{C-m^3}$	$\frac{1}{m^4}$
$m = 2$	$W_\perp$	$\frac{V}{C-m^4}$	$\frac{1}{m^5}$
	W_z	$\frac{V}{C-m^5}$	$\frac{1}{m^6}$

B. Wake Potentials for Charge Distributions

The delta-function wake fields or wake potentials for a point charge, discussed in the previous section, can be used as Green's functions to compute the longitudinal and transverse potentials in an arbitrary charge distribution $I(t)$. Thus for the important case of the longitudinal accelerating mode, the single bunch beam loading potential at time t within the bunch is given by

$$E_b(t) = \int_{-\infty}^{t} W_z(t-\tau)\, I(\tau)\, d\tau \quad . \tag{44}$$

If this expression is divided by the charge, the potential in the bunch per unit charge per unit length (or the potential per discrete component) is obtained. This integrated potential, or bunch potential, is sometimes also called the wake potential. It is unfortunate that the terms "wake potential" and "wake field" are used to refer to several different quantities. The reader is cautioned to check the precise meaning of these terms in each case.

The integrated wake potential for the SLAC structure is shown in Fig. 12 for three different bunch lengths. The total energy gain of a particle at time t in the distribution is then obtained by a superposition of the single bunch beam loading potential per unit length, given by Eq. (44), and the RF accelerating field produced by the external RF source:

$$E(t) = G\cos(\omega t - \theta) - E_b(t) \quad . \tag{45}$$

Here G is the unloaded peak accelerating gradient and θ is the phase angle by which the bunch center leads the crest of the accelerating wave. The total energy spread within the bunch can be minimized by adjusting θ, as described previously.

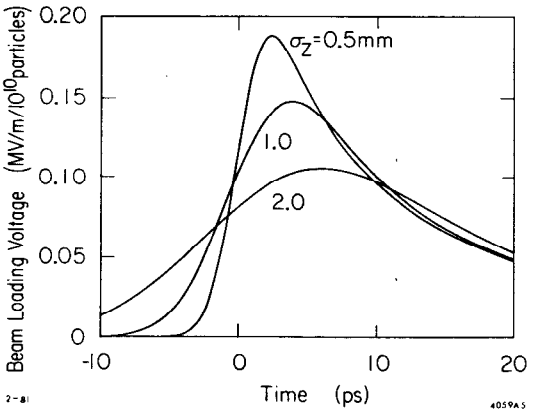

Fig. 12. Beam loading gradient within a single bunch for the SLAC disk-loaded structure. Gaussian bunches of 10^{10} particles, centered at $t = 0$, are assumed.

An additional parameter of interest is the total loss parameter, k_{tot}, given by

$$k_{tot} = \frac{1}{q^2} \int_{-\infty}^{\infty} I(t)\, E_b(t)\, dt \quad . \tag{46}$$

If $E_b(t)$ is the integrated wake due to a single normal mode, it can be shown that, for a Gaussian bunch,

$$k_{tot}(n) \;=\; k_n\, e^{-\omega_n^2\sigma^2} \quad , \tag{47}$$

where $\sigma \;=\; \sigma_z/c$. If $E_b(t)$ is the integrated wake due to all modes, then

$$k_{tot} \;=\; B(\sigma)\, k_1 \quad , \tag{48}$$

where k_1 is the loss parameter for the fundamental mode alone and $B(\sigma)$ is the beam loading enhancement factor. This function is plotted in Fig. 13 for the SLAC structure.

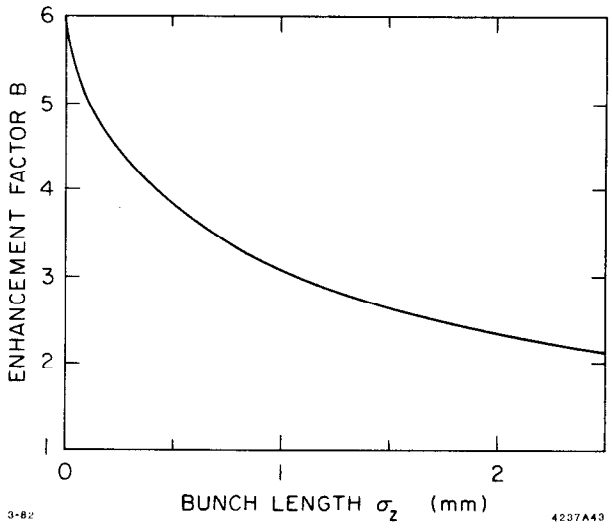

Fig. 13. Single bunch beam loading enhancement factor as a function of bunch length for the SLAC structure.

Functions similar to those defined in Eqs. (44) and (46) for the $m = 0$ case can be constructed using the transverse delta function wake potential $W_\perp(\tau)$. The integrated wake potentials for $m = 0$ and $m = 1$ are compared in Figs. 14 and 15 for the SLAC structure for various bunch lengths[40]. In these two figures, $\mathcal{W}$ is the integrated wake per cell per unit charge. The dashed and solid curves show agreement between the sum of modes method used to calculate the wake, as discussed here, and a direct time integration of Maxwell's equation computed by T. Weiland's code TBCI[41].

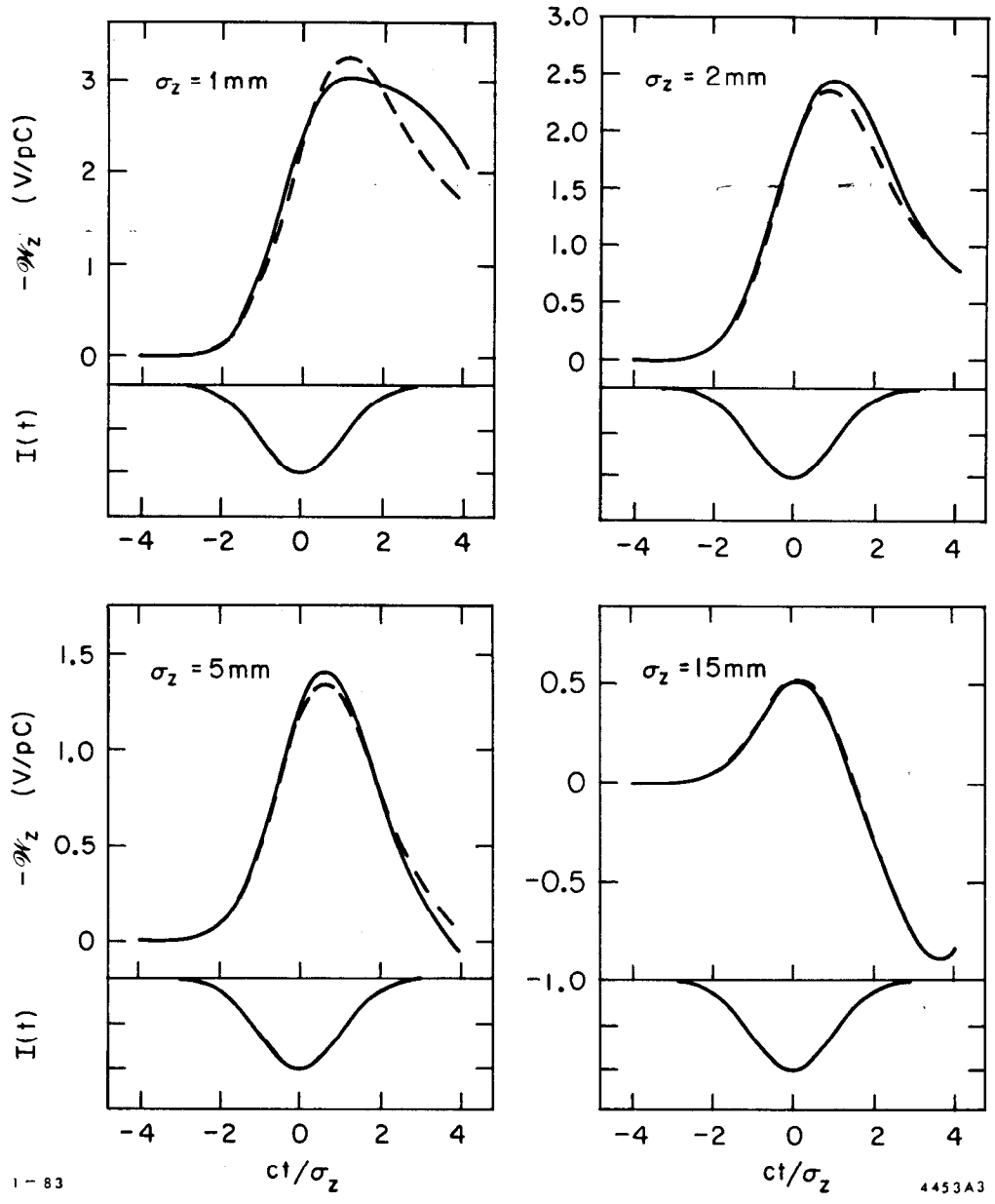

Fig. 14. Longitudinal wake potential ($m = 0$) per cell for gaussian bunches in the SLAC structure. Solid curves give TBCI results and dashed curves are results from a sum of modes.

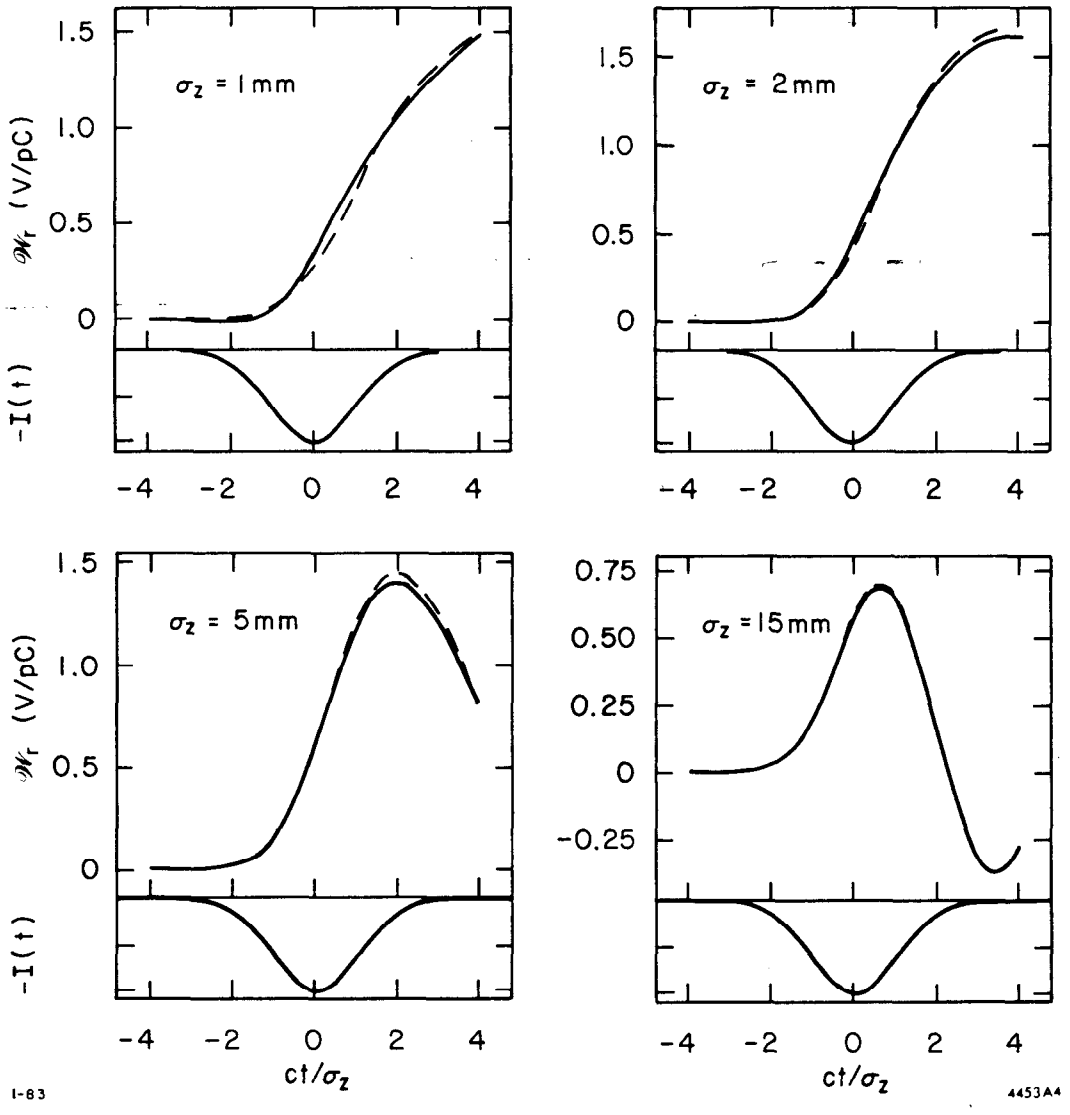

Fig. 15. Transverse wake potential ($m = 1$) per cell for Gaussian bunches in the SLAC structure. Solid curves give TBCI results and dashed curves are results from a sum of modes.

C. Two Particle Model

A simple model in which the bunch current distribution is approximated by two point charges, a leading (head) particle with charge $q/2$ and a following (tail) particle with charge $q/2$, is very useful in estimating emittance growth due to dipole wake field effects in a linac. Consider the simplest case of a linac with constant energy and constant focusing strength $k = 1/\beta$, where $2\pi\beta$ is the

wavelength of the betatron oscillation in the focusing lattice. The equations of motion of the two particles are

$$x_1'' + k^2 x_1 = 0 \quad , \tag{49a}$$

$$x_2'' + (k + \Delta k)^2 x_2 = C x_1 \quad , \tag{49b}$$

where the subscripts 1 and 2 refer to the head and tail particles respectively. Here the prime indicates dx/dz and $C = eqW_1/2E_0$, where W_1 is the dipole wake potential at the position of the trailing charge. (The separation of the two charges can be approximated by $2\sigma_z$). There may also be an energy spread in the bunch due to the longitudinal wake, or to the slope of the RF wave if the bunch is placed off crest. This energy spread can be modelled in the two particle approximation by an energy difference ΔE between the particles, leading to a difference in focusing force $\Delta k/k = \xi \Delta E/E_0$, where ξ is the chromaticity of the lattice (for a lattice with 90° phase shift per cell $\xi = -4/\pi$). For the leading particle, the solution to Eq. (49a) is

$$\tilde{x}_1 = \tilde{x}_{10}\, e^{ikz} \quad , \tag{50}$$

where $\tilde{x}_1$ is a complex quantity giving the amplitude and phase of the oscillation at position z, and $\tilde{x}_{10}$ is the initial value at $z = 0$. If $\Delta k = 0$, the tail particle obeys

$$\tilde{x}_2 = \tilde{x}_{20}\, e^{ikz} - \frac{iCz}{2k}\, \tilde{x}_{10}\, e^{ikz} \quad . \tag{51}$$

Here the first term represents a free betatron oscillation and the second term an oscillation driven by the head particle. If $\tilde{x}_{20} = \tilde{x}_{10}$, the difference $\widetilde{\Delta x} = \tilde{x}_2 - \tilde{x}_1$, grows in amplitude as

$$\left| \frac{\Delta x}{x_{10}} \right| = \frac{Cz}{2k} = \frac{eqW_1 z}{4kE_0} \quad . \tag{52a}$$

In Gaussian units this becomes

$$\frac{\Delta x}{x_{10}} = \frac{r_0 N W_1 z}{4k\gamma} \quad . \tag{52b}$$

If there is an energy difference between the head and tail particles (Landau damping), the solution for x_2 is[14]

$$\tilde{x}_2 = \tilde{x}_{20}\, e^{i(k+\Delta k)z} - \frac{iC\tilde{x}_{10}}{k\Delta k} \sin\left(\frac{z\Delta k}{2}\right) e^{i\left(k+\frac{\Delta k}{2}\right)z} \quad . \tag{53}$$

Again assuming $\tilde{x}_{20} = \tilde{x}_{10}$, the difference $\widetilde{\Delta x} = \tilde{x}_2 - \tilde{x}_1$, grows in amplitude as

$$\left| \frac{\Delta x}{x_{10}} \right| = 2\left(1 - \frac{C}{2k\Delta k}\right) \sin\left(\frac{z\Delta k}{2}\right) \quad . \tag{54}$$

As has been pointed out[14], the emittance growth is zero if either $z\Delta k = 2n\pi$ or if $C = 2k\Delta k$. This latter condition can be written, for a 90° lattice,

$$\Delta E = -\frac{\pi e q W_1}{16k^2} \quad . \tag{55}$$

However, even in the worst case the amplitude does not exceed $C/k\Delta k$, which becomes for a 90° lattice

$$\frac{\Delta x}{x_{10}} < -\frac{\pi e q W_1}{8k^2 \Delta E} \quad . \tag{56}$$

The amplitude of the wake potential W_1 can be determined from Fig. 10, at least approximately, by taking the wake potential at distance σ_z behind the bunch center. Thus for a 1 mm bunch in the SLAC structure $W_1 \approx 0.8$ V/pC/cell, or 2×10^{15} V/C-m^2. In Gaussian units this becomes $W_1 = 2 \times 10^5/\text{m}^3$.

VI. EMITTANCE

A. General Remarks

The scaling laws in Sec. II show that very small emittance beams will be required for future linear colliders operating in the energy range above 1 TeV. The normalized emittance required for a 5 TeV machine, for example, might be on the order of 10^{-7}–$10^{-8}\,\pi$ m-rad.[42]. In this section some limitations and expectations concerning the emittance that can be obtained from linac injectors and damping rings will be briefly discussed.

Linear optics and emittance concepts in beam transport systems and in circular machines have been discussed in several tutorial papers.[43] We are concerned here with periodic linear transport systems, and for this case a word of caution is in order. In a circular machine, the lattice functions (*e.g.*, β) are truly periodic and can be defined by the characteristics of the focusing lattice alone, even where no beam is present. This is not the case for a linear transport system. Assume that the transport system consists of a finite number of identical cells. The initial beam ellipse in the phase plane at the entrance to the first cell must still be defined in order to define the initial values of the lattice functions. Alternatively, the values at the end of the last cell could also be defined by working back from the final focus. Expressed differently, the concept of a beta function in a linear collider is only meaningful if the beam ellipse is defined at some location in the transport system.

B. Emittance from Guns

The emittance of a typical linac injector is for the most part determined by the emittance of the gun itself. Consider a point on the surface of a hot cathode. Electrons leaving this point have a transverse momentum proportional to $(KT)^{1/2}$, where K is the Boltzmann constant. The transverse emittance is then proportional to this momentum times the radius of the cathode, or to the square root of the cathode area. For a fixed current density, the area is in turn proportional to the total current. Thus, it is reasonable to write

$$\epsilon_n = \gamma\epsilon \approx 1 \times 10^{-4} \sqrt{\hat{I}B}\ \pi \text{ m-rad} \quad , \tag{57}$$

where $\hat{I}$ is the peak current in the bunch in amperes and B is the bunching factor. This expression is also called the Lawson–Penner relation (see, for example, Ref. 44).

In addition to the transverse momentum due to the finite temperature of the cathode, other factors contribute to the beam emittance in the gun region. These factors include field fringing at grid and anode apertures, nonlinear forces in focusing lenses, and transverse RF fields which vary longitudinally over the bunch in the bunching region. A number of suggestions have been made for reducing or eliminating these deleterious effects, such as: removal of grids, very high gun voltages, tight focusing, bunching at high energy, use of a cathode in which the emission is driven by a microwave field, and photocathodes in which the emission is driven by a modulated laser beam.

The normalized emittance for typical present-day linacs at 100 A peak cathode current is the range of 1–3 $\times 10^{-4}\,\pi$ m-rad. It is expected that this can be reduced by a factor of ten or so in the case of a laser-driven photocathode. The thermal limit lies still another order of magnitude lower.

C. Emittance from Damping Rings

Low emittance storage rings are of interest as synchrotron radiation sources, as beam recirculation devices for FELs, and as injectors for linear colliders. Assume first a ring with a lattice consisting of bending magnets of length $\ell = \rho\theta$, with a waist in the β function at the center of each magnet and appropriate focusing elements between the magnets. Then it can be shown[45] that the minimum normalized emittance is given by

$$\epsilon_n = 8.3 \times 10^{-15}\, \gamma^3\, \theta^3\, \pi \text{ m-rad} \quad . \tag{58a}$$

The more conventional FODO lattice produces a considerably higher minimum normalized emittance, given by[46]

$$\epsilon_n \;=\; \frac{4.8\times 10^{-13}}{F_m}\,\gamma^3\,\theta^3\,\pi\ \text{m-rad}\quad , \tag{58b}$$

where F_m is the fraction of the ring filled by the magnets. From the standpoint of low emittance, therefore, a damping ring should consist of a large number of very short bending magnets with a large bending radius.

It is natural to ask whether there is a fundamental limit on the emittance that can be achieved using this strategy. It is clearly not productive to reduce the bending angle below the opening angle for synchrotron radiation. More precisely, it can be shown[47] that $\theta_{min} \approx 6/\gamma$. Using this in Eq. (58a),

$$\epsilon_n \;\approx\; 1.8\times 10^{-12}\,\pi\ \text{m-rad}\quad . \tag{59}$$

In addition to emittance, other factors must be considered in the design of a damping ring. For either lattice, the damping rate is given by[46]

$$[\tau\,(\text{sec})]^{-1} \;=\; 2.1\times 10^{-3}\,F_m\,E_0^3\,(\text{GeV})\,\Big/\,\rho^2\,(\text{m})\quad . \tag{60}$$

Thus for a fast damping rate, required for a collider with a high repetition rate, a small bending radius is desirable. This is in conflict with the requirement for low emittance, and a compromise must be struck.

The Touschek effect may limit the beam lifetime is a storage ring designed for low emittance, and intrabeam scattering (multiple Touschek effect) may produce emittance growth. In a damping ring the beam lifetime needs to be only a few damping times, and the limitation on lifetime imposed by the Touschek effect is normally not of concern. Intrabeam scattering, however, may impose a serious limitation on emittance. It is difficult to write a precise relation giving the scaling for this effect, but the threshold current at which significant emittance growth becomes observable increases rapidly with increasing energy. Computer programs[48] are available for calculating beam lifetime limitations and emittance growth due to intrabeam scattering in storage rings designed for high brightness synchrotron radiation sources and FELs. For these applications, normalized emittances on the order of $5\times 10^{-6}\,\pi$ m-rad have been achieved. This is a factor of six lower than the emittance of the SLC damping ring at SLAC ($\epsilon_n = 3\times 10^{-5}$). For a 5 TeV collider, an emittance which is still lower by two or three orders of magnitude may be required. However, a serious effort to design damping rings capable of producing beam emittances of this order is only just beginning.

Acknowledgment

The help of P. Morton and L. Rivkin in preparing Sec. VI is gratefully acknowledged.

References

1. Ugo Amaldi, ed., Proc. of the 2nd ICFA Workshop on Possibilities and Limitations of Accelerators and Detectors, Les Diablerets, Switzerland, October 1979 (CERN, June 1980), pp. 3–20.
2. H. Wiedemann, 1981 SLAC Summer Institute on Particle Physics, SLAC–PUB–2849 (November 1981).
3. R. Hollebeek, Nucl. Instrum. Methods **184**, 333 (1981).
4. W. M. Fawley and E. P. Lee, UCID–18584, Lawrence Livermore Laboratory (1980).
5. R. Noble, private communication.
6. M. Bassetti and M. Gygi–Hanney, LEP–Note–221, CERN, Geneva (1980).
7. T. Erber and G. B. Baumgartner Jr., Proc. 12th Int. Conf. on High Energy Accelerators (Fermilab, August 1983), p. 372.
8. T. Himel and J. Siegrist, "Quantum Effects in Linear Collider Scaling Laws." These Proceedings.
9. P. B. Wilson, "High Energy Electron Linacs: Applications to Storage Ring RF Systems and Linear Colliders," in *Physics of High Energy Accelerators,* R. A. Carrigan, F. R. Huson and M. Month, eds. (AIP Conf. Proc. No. 87, New York, 1982); also SLAC–PUB–2884. (See Sec. 10.1.)
10. See Ref. 9, Sec. 12.3.
11. A. N. Skrinsky, Proc. 12th Int. Conf. on High Energy Accelerators (Fermilab, August 1983), p. 104.
12. A. Chao, SLAC Internal Note (May 1983).
13. A. Chao and L. Rivkin, SLAC Internal Note CN–263 (January 1984).
14. K. L. F Bane, "Landau Damping in the SLAC Linac," 1985 Particle Accelerator Conf. (to be published in IEEE Trans. Nucl. Sci. **NS-32**); also SLAC–PUB–3670.
15. See, for example, Ref. 9, Sec. 10.1.
16. E. L. Garwin *et al.,* "An Experimental Program to Build a Multimegawatt Lasertron for Super Linear Colliders," 1985 Particle Accelerator Conf. (to be published in IEEE Trans. Nucl. Sci. **NS–32**); also SLAC–PUB–3650.
17. W. D. Kilpatrick, Rev. Sci. Instr. **28**, 824 (1957).

18. G. Konrad, private communication.

19. R. B. Miller, *An Introduction to the Physics of Intense Charged Particle Beams* (Plenum Press, New York, 1982), p. 11.

20. G. Loew and J. Wang, "Measurement of Ultimate Accelerating Gradients in the SLAC Disk–Loaded Structure." 1985 Particle Accelerator Conf. (to be published in IEEE Trans. Nucl. Sci. **NS-32**); also SLAC–PUB–3597.

21. Eiji Tanabe, IEEE Trans. Nucl. Sci. **NS–30, No. 4**, 3551 (1983).

22. V. L. Granatstein, 1984 Summer School on High Energy Particle Accelerators, Fermilab (to be published in AIP Conf. Proc.).

23. Rome Air Development Center, Report RADC–TR–70–101 (July 1970).

24. T. G. Lee *et al.*, "The Design and Performance of a 150 MW Klystron at S–Band" (to be published in IEEE Trans. Plasma Science.); also SLAC-PUB–3619.

25. V. L. Granatstein, to be published in Int. J. Electronics **57** (1984).

26. Y. Fukushima *et al.*, "Lasertron, a Photocathode Microwave Device Switched by Laser." 1985 Particle Accelerator Conf. (to be published in IEEE Trans. Nucl. Sci. **NS-32**).

27. W. Herrmannsfeldt, SLAC–AP/41 (May 1985).

28. Z. D. Farkas, "Binary Power Multiplier." Submitted to MTT Special Transactions Issue on New and Future Applications of Microwave Systems, to be published October 1986. Also SLAC–PUB–3694.

29. K.L.F Bane, Pisin Chen and P. B. Wilson, "On Collinear Wake Field Acceleration," 1985 Particle Accelerator Conf. (to be published in IEEE Trans. Nucl. Sci. **NS-32**); also SLAC–PUB–3662.

30. G. Voss and T. Weiland, DESY Report 82–074 (November 1982).

31. T. Weiland, "Wake Field Work at DESY," 1985 Particle Accelerator Conf. (to be published in IEEE Trans. Nucl. Sci. **NS-32**).

32. J. Wurtele, " On Acceleration by the Transfer of Energy between Two Beams," these Proceedings.

33. A. M. Sessler, "The Free Electron Laser as a Power Source for a High Gradient Structure," in *Laser Acceleration of Particles,* P. J. Channell, ed. (AIP Conf. Proc. No. 91, New York, 1982), pp. 163–189.

34. Suggested by W.K.H. Panofsky.

35. Ref. 9, Sec. 9.

36. A. W. Chao, "Coherent Instabilities of a Relativistic Bunched Beam," in *Physics of High Energy Particle Accelerators,* M. Month, ed. (AIP Conf. Proc. No. 105, New York, 1983), pp. 353–523.

37. K. L. F. Bane, P. B. Wilson and T. Weiland, "Wake Fields and Wake Field Acceleration" in *Physics of High Energy Particle Accelerators*, M. Month, Per F. Dahl and M. Dienes, eds. (AIP Conf. Proc. No. 127, New York, 1985), pp. 875-928.

38. K. L. F. Bane and R. K. Cooper, Invited Lectures at the 1984 Summer School on High Energy Particle Accelerators (to be published in AIP Conf. Proc).

39. K. L. F. Bane, private communication.

40. K. Bane and T. Weiland, SLAC/AP-1 (January 1983).

41. T. Weiland, 11th Int. Conf. on High Energy Accelerators (Birkhäuser Verlag, Basel, 1980), pp. 570–575.

42. B. Richter, "Requirements for Very High Energy Accelerators," these Proceedings.

43. See, for example, K. L. Brown and R. V. Servranckx, "First and Second Order Charged Particle Optics," in *Physics of High Energy Particle Accelerators,* M. Month, Per F. Dahl and M. Dienes, eds. (AIP Conf. Proc. No. 127, New York, 1985), pp. 62–138.

44. L. R. Elias and G. J. Ramian, "Status Report of the UCSB FEL Experimental Program," in *Free-Electron Generators of Coherent Radiation,* C. A. Brau, S. F. Jacobs and M. O. Scully, eds., Proc. SPIE **453**, 137 (1984).

45. L. C. Teng, internal report LS–17, Argonne National Laboratory (March 1985); also internal report TM–1269, Fermilab (June 1984).

46. H. Wiedemann, 11th Int. Conf. on High Energy Accelerators (Birkhäuser Verlag, Basel, 1980), p. 693.

47. L. Rivkin, private communication

48. Computer code ZAP by M. S. Zisman, J. Bisognano and S. Chattopadhyay, Lawrence Berkeley Laboratory. Unpublished.

49. K–J. Kim *et al.,* "Storage Ring Design for a Short Wavelength FEL," 1985 Particle Accelerator Conf. (to be published in IEEE Trans. Nucl. Sci. NS-**32**).